JHEP

Published for SISSA by Springer

Received: November 10, 2021
Revised: February 22, 2022
Accepted: March 21, 2022
Published: April 6, 2022

Heavy long-lived coannihilation partner from inelastic Dark Matter model and its signatures at the LHC

Jinhui Guo,[a] **Yuxuan He,**[a] **Jia Liu**[a,b] **and Xiao-Ping Wang**[c,d]

[a] *School of Physics and State Key Laboratory of Nuclear Physics and Technology, Peking University, Beijing 100871, China*

[b] *Center for High Energy Physics, Peking University, Beijing 100871, China*

[c] *School of Physics, Beihang University, Beijing 100083, China*

[d] *Beijing Key Laboratory of Advanced Nuclear Materials and Physics, Beihang University, Beijing 100191, China*

E-mail: guojh23@pku.edu.cn, heyx25@pku.edu.cn, jialiu@pku.edu.cn, hcwangxiaoping@buaa.edu.cn

Abstract: The coannihilation mechanism is a well-motivated alternative to the simple thermal freeze-out mechanism, where the dark matter relic density can be obtained through the coannihilation with a partner particle of similar mass with dark matter. When the partner particle is neutral, the inelastic nature of dark matter can help it to escape the direct detection limits. In this work, we focus on the coannihilation scenario in which the annihilation cross section is dominated by the partner-partner pair annihilation. We pay special interest on the parameter space where the coannihilation partner is long-lived, which leads to displaced signatures at the collider. In such case, it opens the heavy mass parameter space for the coannihilation dark matter, comparing with those dominated by the partner-dark matter annihilation. Specifically, we study an inelastic scalar dark matter model with a specific parameter space, which realizes the domination of partner-partner pair annihilation. Then, we study two different realizations of the coannihilation partner decay and the existing constraints from the relic abundance, direct and indirect dark matter detection and the collider searches. We focus on the channel that the long-lived coannihilation partner decays to dark matter plus leptons. The high-luminosity LHC can reach good sensitivities for such heavy dark matter and coannihilation partner around 100–700 GeV.

Keywords: Beyond Standard Model, Higgs Physics

ArXiv ePrint: 2111.01164

https://doi.org/10.1007/JHEP04(2022)024

JHEP04(2022)024

Contents

JHEP04(2022)024

1 Introduction

The dark matter (DM) is a fundamental and unresolved problem of the particle physics, given the great triumph of the Standard Model (SM) in explaining the phenomenons observed in local laboratories and the astrophysical studies. The Weakly Interacting Massive Particle (WIMP) scenario is one of the most popular dark matter models, which can explain the dark matter relic abundance, $\Omega h^2 = 0.1198 \pm 0.0026$ [1], through its thermal freeze-out mechanism with a weak scale annihilation cross section. It hints new physics could be related with weak scale or higher. The scenario can be cross-checked using the large hadron collider (LHC), terrestrial direct searches of the DM particles and indirect searches for the DM annihilation products. Until now, dark matter escapes all the above searches and people start to think about alternatives.

The coannihilation mechanism is one of the possible alternatives [2], where the dark matter coupling to the SM particles can be quite small. As a result, the dark matter pair annihilation cross section is small, which helps it to evade the strong constraints on the dark matter pair annihilation from the Cosmic Microwave Background (CMB) [1, 3] and the indirect searches [4–8]. Due to the small coupling to SM particles, the direct searches constraints at deep underground experiments can also be safely evaded [9–12]. In the coannihilation scenario, its relic abundance is obtained through the annihilation with a slightly heavier particle, denoted as the *coannihilation partner*. In general, it will decay back to the dark matter particle. If the coupling and the mass splitting to dark matter are small enough, it can be a long-lived particle (LLP) at the detector scale [13]. Different from the DM, the coannihilation partner can have a sizable coupling to SM particles to obtain a large

coannihilation cross section. Therefore, it is possible for LHC to produce an abundance of the coannihilation partners. However, the detection might be difficult, for example, if the mass splitting is too small, the visible decay products of the coannihilation partner are too soft to detect. If the coannihilation particle is charged under the SM gauge group, the partner can have significant interactions to the SM particles, such as in supersymmetric models [14–16] and in many simplified models [17–21]. The LHC can probe those charged coannihilation particles via disappearing tracks, which has been studied in refs. [22, 23].

If the coannihilation partners are not charged under the SM gauge group, then they are *neutral* coannihilation partners. The neutral partners could come from the same origin as the dark matter, for example the inelastic dark matter (iDM), coming from a degenerate mass spectrum and later splitting into two separate states [24]. More specifically, the ultraviolet model starts with a complex scalar or Dirac fermion dark matter, which can be charged under a dark sector $\mathrm{U}(1)_D$, and then splits into the dark matter state DM_1 and the excited state DM_2. The dark gauge boson A' dominantly couples to $\mathrm{DM}_1 + \mathrm{DM}_2$, while the diagonal couplings to $\mathrm{DM}_1 + \mathrm{DM}_1$ and $\mathrm{DM}_2 + \mathrm{DM}_2$ are vanishing or suppressed by the small mass splitting [24, 25]. These neutral coannihilation particles can be probed via the long-lived signatures, which has been done at Belle-II and LHC [26–29]. One can also look for them at future LHC, neutrino programs and fixed target experiments [27, 30, 31].[1]

In this work, we study the LLP signatures from a scalar iDM model at the LHC. In our setup, we consider the dark matter and coannihilation particles coming from a complex scalar. The complex scalar can couple to SM Higgs directly through the scalar quartic coupling, which effect is less studied for coannihilation partner in the previous literature. Previously, people usually focused on the Higgs portal dark matter for a singlet scalar dark matter or a complex scalar dark matter, with a scalar quartic coupling like $s^2 H^\dagger H$ or $S^* S H^\dagger H$ [34–41]. Such dark matter model is heavily constrained by the direct detection experiments [42–48], especially the recent results from XENON1T [11] and PandaX [12, 49, 50], leaving only the resonance region viable. Different from Higgs portal dark matter model, a singlet coannihilation scalar will open the parameter space from DM direct detection [51–54], via significant coannihilation contribution.

In general, there are three kinds of coannihilation processes: $\mathrm{DM}_1 + \mathrm{DM}_1$, $\mathrm{DM}_1 + \mathrm{DM}_2$, and $\mathrm{DM}_2 + \mathrm{DM}_2$. Most of previous coannihilation studies [26–31] focus on the coannihilation process $\mathrm{DM}_1 + \mathrm{DM}_2$.[2] In this case, a small coupling between DM and coannihilation partner is necessary to make the partner long-lived. Therefore, one has to lower the DM mass scale to compensate this small coupling for the relic abundance. As a result, the DM mass has to be lighter than 100 GeV. However, our coannihilation partner couples to SM Higgs via the scalar quartic, we can have a large $(\mathrm{DM}_2 + \mathrm{DM}_2)$ partner pair annihilation cross section (σ_{22}). Later, we will build an ultraviolet model for the specific quartic coupling from a broken symmetry. In our setup, the coannihilation partner (DM_2) couples to the SM Higgs, while the dark matter (DM_1) does not couple to SM Higgs directly, which is different to the Higgs portal DM model. In our model, the DM pair annihilation cross

[1] It is also worth mentioning that the iDM with large mass splitting can be used to reopen the kinetic mixing dark photon parameter space for $(\text{g-2})_\mu$ anomaly [32, 33].

[2] Ref. [55] considered the process $\mathrm{DM}_2 + \mathrm{DM}_2$ but only for very light DM.

JHEP04(2022)024

section σ_{11} is vanishing. The DM-partner annihilation cross section σ_{12} is sub-dominant in the contribution of relic abundance, which separates our study from the previous ones. Since the relic abundance is fulfilled by the coannihilation partner pair annihilation, we can focus on much larger dark matter mass region ($> 100\,\text{GeV}$), where the decay products are much more energetic than light DM scenario. As a result, in our work, the annihilation channels for relic abundance, production channel at collider and DM mass region are quite different from the previous studies. Next we study the existing constraints for this model from collider, direct and indirect searches. Later, we will study an ultraviolet model in a specific parameter space, which leads to a special quartic coupling.

We organize the paper as follows. In section 2, we describe the scalar inelastic dark matter models and the possible decay channels for the long-lived coannihilation partner. In section 3, we discuss the existing constraints from dark matter relic abundance, direct detection, indirect detection and collider searches. In section 4, we discuss the long-lived particle signatures of the coannihilation partner and its detection at the LHC. In section 5, we conclude.

2 The models

The coannihilation mechanism can contribute significantly to the DM relic abundance. For this purpose, the coannihilation partner number density should be comparable to the DM. As a result, its mass can not be too large comparing with DM. In our study, we consider a complex scalar iDM model, with the real scalar ground state s_1 and excited state s_2 as the coannihilation partner. The dimensionless mass splitting between s_1 and s_2 is defined as

$$\Delta \equiv \frac{m_2 - m_1}{m_1}, \tag{2.1}$$

where $m_{1,2}$ are the mass for $s_{1,2}$. If assuming the density ratio between s_1 and s_2 follows the equilibrium value, one can solve the Boltzmann equation and obtain an effective cross section [2, 15, 17, 56]

$$\sigma_{\text{eff}} = \frac{g_{s_1}^2}{g_{\text{eff}}^2}\left(\sigma_{11} + 2\sigma_{12}\frac{g_{s_2}}{g_{s_1}}(1+\Delta)^{3/2}e^{-x\cdot\Delta} + \sigma_{22}\frac{g_{s_2}^2}{g_{s_1}^2}(1+\Delta)^3 e^{-2x\cdot\Delta}\right), \tag{2.2}$$

where $\sigma_{ij} = \sigma(s_i\ s_j \to \text{SM SM})$ is the annihilation cross section to SM particles, $g_{s_1} = g_{s_2} = 1$ are the degrees of freedom for real scalar s_1 and s_2, and $x = m_{\text{DM}}/T$ where T is the temperature of thermal bath. The effective degree of freedom g_{eff} is defined as

$$g_{\text{eff}} = g_{s_1} + g_{s_2}(1+\Delta)^{3/2}e^{-x\cdot\Delta}.$$

When the cross section σ_{11} is negligible, the dominant contributions to effective cross section σ_{eff} come from the coannihilation. The previous studies focused on the case that σ_{12} is the dominant contribution to the effective annihilation cross section. We consider an alternative case that the coannihilation DM model leads to the following annihilation cross section,

$$\sigma_{11} \approx 0, \quad \sigma_{12} \ll \sigma_{22}. \tag{2.3}$$

JHEP04(2022)024

It can enable us to consider the heavy DM parameter space and more energetic decay objects from long-lived s_2. The concrete model satisfying this feature will be introduced in the following subsection.

2.1 Inelastic scalar dark matter model

We start with the Lagrangian for a massive complex scalar $\hat{S}$, which satisfies a global U(1) symmetry,

$$\mathcal{L}_{\mathrm{U}(1)} = \left(\partial_\mu \hat{S}\right)^* \left(\partial^\mu \hat{S}\right) - m_S^2 \hat{S}^* \hat{S}, \tag{2.4}$$

where $\hat{S} = (\hat{s}_1 + i\hat{s}_2)/\sqrt{2}$ is a complex scalar and $\hat{s}_{1,2}$ are the real scalars. The notation with a hat, e.g. $\hat{S}$, is for flavor eigenstates, and we reserve the notation without a hat for mass eigenstates. Then we add a quadratic term $\hat{s}_i \hat{s}_j$ into the Lagrangian $\mathcal{L}_{\cancel{\mathrm{U}(1)}}$ to explicitly break the U(1) symmetry:

$$\mathcal{L}_{\cancel{\mathrm{U}(1)}} = -\delta\hat{m}^2_{ij}\hat{s}_i\hat{s}_j - \hat{\lambda}_{ij}\hat{s}_i\hat{s}_j\left(H^\dagger H - \frac{v^2}{2}\right), \tag{2.5}$$

where H is the SM Higgs doublet and v is the SM Higgs vacuum expectation value (vev). The mass matrix $\delta\hat{m}^2$ and scalar quartic coupling matrix $\hat{\lambda}$ are real symmetric matrices. We neglect other self-interacting quartic scalar terms which are irrelevant in this work.

To obtain the mass eigenstates, one can apply a U(1) rotation U, parameterized with an angle θ,

$$U = \begin{pmatrix} \cos\theta & \sin\theta \\ -\sin\theta & \cos\theta \end{pmatrix}, \tag{2.6}$$

which transfers the U(1) eigenstates to the mass eigenstates and diagonalizes the mass matrix via

$$\begin{pmatrix} \hat{S}_1 \\ \hat{S}_2 \end{pmatrix} = U \begin{pmatrix} S_1 \\ S_2 \end{pmatrix}, \quad U^\dagger \cdot \delta\hat{m}^2 \cdot U = \begin{pmatrix} \delta m_{11}^2 & 0 \\ 0 & \delta m_{22}^2 \end{pmatrix}. \tag{2.7}$$

Since the components proportional to identity matrix, $\delta m_{11}^2 \times I$, can be absorbed into the U(1) conserving mass term $m_S^2 \hat{S}^\dagger \hat{S}$, we can set $\delta m_{11}^2 = 0$ without loss of generality. Because the Lagrangian $\mathcal{L}_{\mathrm{U}(1)}$ is invariant under the rotation U, we obtain the Lagrangian in the mass eigenstates with DM mass and excited states mass respectively,

$$m_1^2 = m_S^2, \quad m_2^2 = m_S^2 + \delta m_{22}^2, \tag{2.8}$$

where $\delta m_{22}^2 > 0$ is chosen, making s_2 the excited state.

The diagonalization of the mass matrix $\delta\hat{m}^2$ breaks the U(1) global symmetry from random rotation to a special rotation angle θ. Furthermore, the mass matrices $\delta\hat{m}^2$ and δm^2 are rank one, because $\delta m_{11}^2 = 0$. It contributes a massive term $\delta m_{22}^2 s_2 s_2$ to the Lagrangian, while keeps s_1 mass unchanged. In the aspect of global symmetry breaking, s_2 is similar to a radial mode, while s_1 is similar to the Goldstone mode after the symmetry breaking. Actually, the special mass term δm^2 can be obtained by adding another complex scalar ϕ and assigning the global U(1) charge -2 to ϕ and charge 1 to $\hat{S}$. Therefore, there is a new interaction term can be written as

$$\mu\phi\hat{S}\hat{S} + h.c., \tag{2.9}$$

JHEP04(2022)024

and the special rotation angle θ is actually

$$\theta = \frac{1}{2}\arg\left[\mu \times \langle\phi\rangle\right], \tag{2.10}$$

where $\langle\phi\rangle$ is the vev which explicitly breaks the global U(1). After appropriately subtracting the identity component, one can obtain the required rank one mass matrix.

In principle, for the scalar quartic coupling $\hat{\lambda}_{ij}\hat{s}_i\hat{s}_j H^\dagger H$, it can exist the U(1) conserving component $|S|^2 H^\dagger H$, which can couple both $s_1 s_1$ and $s_2 s_2$ to the SM Higgs. However, it will make DM pair annihilation cross-section σ_{11} comparable to the coannihilation partner annihilation cross-section σ_{22} and the scenario comes back to the normal DM freeze-out. Therefore, we will omit the above parameter space and focus on the specific parameter space where $s_1 s_1$ does not couple to $H^\dagger H$. Technically, it can be realized by adding the higher dimensional operator $\alpha\phi\hat{S}\hat{S}H^\dagger H + h.c.$ and *require* that the complex phases of α and μ are the same. In this case, the matrix $\hat{\lambda}$ is aligned with the special rotation angle ϕ and only $s_2 s_2$ couples to $H^\dagger H$. We emphasize that the U(1) conserving component $|S|^2 H^\dagger H$ also respects the special rotation but is forbidden by hand. Therefore, the above procedure actually picks up a specific interaction and leads to the parameter space which we are interested in. As a result, the following effective Lagrangian is our baseline model and in the mass eigenstates it reads,

$$\mathcal{L}_{\text{eff}} = \left(\partial_\mu S\right)^\dagger \left(\partial^\mu S\right) - \frac{m_1^2}{2}s_1^2 - \frac{m_2^2}{2}s_2^2 - \lambda_{22}s_2^2\left(H^\dagger H - \frac{v^2}{2}\right). \tag{2.11}$$

This is the scalar iDM model to start with. It provides the mass splitting between dark matter ground state s_1 and exited state s_2, and fulfills the requirement in eq. (2.3). In eq. (2.11), there is no interaction between s_1 and s_2 yet, to provide the decay of s_2. We will introduce two models for the decay of s_2 in the next subsection.

2.2 The excited dark matter particle as long-lived particle

Starting from the effective Lagrangian $\mathcal{L}_{\text{eff}}$, we have zero ground state annihilation $\sigma_{11} = 0$ and the coannihilation is dominant by σ_{22}. However, we should introduce a coupling between s_1 and s_2, because s_1 has to be in thermal equilibrium with s_2 and the SM thermal bath. In addition, the coupling has to be small to make s_2 long-lived at the collider detector scale. We provide two models to achieve the above requirements.

Pure-Scalar model (PS): we do not add new particles but slightly break the specialty of the angle θ. Specifically, the mass matrix $\delta\hat{m}^2$ and interaction matrix $\hat{\lambda}$ can commute with each other, $\left[\delta\hat{m}^2,\ \hat{\lambda}\right] = 0$, thus they can be simultaneously diagonalized by a rotation matrix U. It means both matrices align to rotation angle θ. Once the interaction is slightly misaligned to $\theta + \delta\theta$ with $\delta\theta \ll \theta$, there are regenerated interactions between s_1–s_2 and s_1–s_1 itself

$$\lambda_{12} \approx -\delta\theta \times \lambda_{22}, \quad \lambda_{11} \approx \delta\theta^2 \times \lambda_{22}. \tag{2.12}$$

Since $\delta\theta$ is very small, λ_{12} can lead to a slow decay of s_2. Because λ_{11} is at the order of $\delta\theta^2$ which is negligible, thus the ground state annihilation contributes negligible cross

JHEP04(2022)024

section σ_{11} comparing to the coannihilation. At leading order of $\delta\theta$, we denote the new contribution as the *pure scalar model*

$$\mathcal{L}_{12}^{S} = -\lambda_{12} s_1 s_2 \left(H^\dagger H - \frac{v^2}{2} \right), \tag{2.13}$$

with $\lambda_{12} \ll \lambda_{22}$. Both annihilation process $s_1 s_2 \to \text{SM SM}$ and the decay width of s_2 are suppressed by λ_{12}. Moreover, the decay width of s_2 is additionally suppressed by small mass splitting Δ and small fermions mass in the Yukawa interaction. The s_2 decay width is approximately

$$\Gamma(s_2 \to s_1 f \bar{f}) \simeq \frac{\lambda_{12}^2 m_f^2 m_2^3 \Delta^5}{240\pi^3 m_h^4} \times \theta(m_1 \cdot \Delta - 2m_f), \tag{2.14}$$

where the small mass m_f is taken to be zero in the phase space integration. For a typical electroweak mass, e.g. $m_2 \sim 200\,\text{GeV}$, s_2 has a decay length (with all final decay states considered) of $\mathcal{O}(10\text{ cm})$ for $\lambda_{12} \sim 10^{-3}$ and mass splitting $\Delta \sim 10\%$. For massive m_f comparable to mass splitting, one should numerically integrate the phase space to obtain the decay width.

Scalar-Vector model (SV): we promote the global U(1) to local U(1), and keep the specialty of the rotation θ that $\left[\delta\hat{m}^2,\ \hat{\lambda}\right] = 0$. There is a massive dark photon A', from the $\text{U}(1)_D$ gauge field in the hidden sector, which can connect to SM particles via kinetic mixing term. The effective Lagrangian of DM and the Lagrangian of the dark photon are given below,

$$\mathcal{L}_{\text{eff}} = (D_\mu S)^\dagger (D^\mu S) - \frac{m_1^2}{2} s_1^2 - \frac{m_2^2}{2} s_2^2 - \lambda_{22} s_2^2 \left(H^\dagger H - \frac{v^2}{2} \right), \tag{2.15}$$

$$\mathcal{L}_{A'} = -\frac{1}{4} \hat{F}'^{\mu\nu} \hat{F}'_{\mu\nu} - \frac{\epsilon}{2c_w} \hat{F}'^{\mu\nu} B_{\mu\nu} + \frac{m_{A'}^2}{2} \hat{A}'^{\mu} \hat{A}'_{\mu}, \tag{2.16}$$

where $D_\mu = \partial_\mu - i g_D A'_\mu$ is the covariant derivative for the $\text{U}(1)_D$ interaction. $\hat{F}'$ is the field strength of $\hat{A}'$, B is the field strength of the hypercharge field, ϵ is the strength of kinetic mixing, and c_w is the cosine of the weak angle.

We can use a non-unitary matrix to rotate away the kinetic mixing terms and work in the mass eigenstates as follows at leading order of ϵ [57, 58],

$$\begin{pmatrix} \hat{Z}_\mu \\ \hat{A}_\mu \\ \hat{A}'_\mu \end{pmatrix} = \begin{pmatrix} 1 & 0 & \frac{m_{A'}^2 t_w}{m_Z^2 - m_{A'}^2}\epsilon \\ 0 & 1 & \epsilon \\ \frac{m_Z^2 t_w}{m_{A'}^2 - m_Z^2}\epsilon & 0 & 1 \end{pmatrix} \begin{pmatrix} Z_\mu \\ A_\mu \\ A'_\mu \end{pmatrix}, \tag{2.17}$$

where A, Z and A' are the photon, Z boson in the SM and extra gauge boson from $\text{U}(1)_D$ in the mass eigenstate, while the expressions with a hat are for flavor basis. The rotation matrix is expanded to $\mathcal{O}(\epsilon)$ and the mass m_Z should not be too close to $m_{A'}$. The mixing among dark photon A', Z boson and massless photon gives rise to the coupling of A' to

JHEP04(2022)024

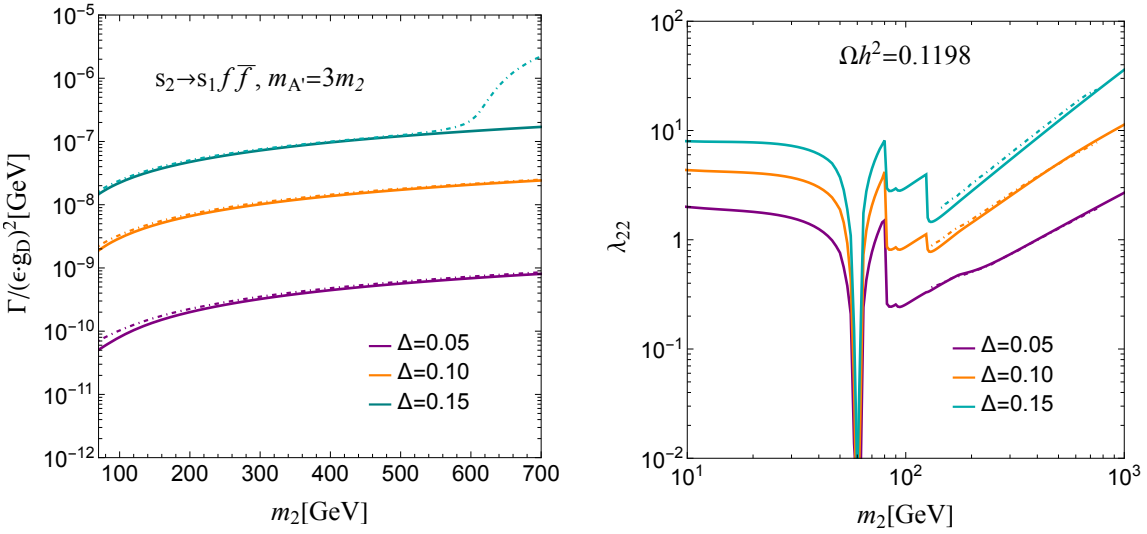

(a) (b)

Figure 1. The left panel (a) shows the coannihilation partner s_2 total decay width ($\Delta = 0.05,\ 0.10$ and 0.15) as a function of its mass m_2. The solid line and dashed line are our approximate and MadGraph results respectively. The dot-dashed cyan line has a difference at large mass for $\Delta = 0.15$, because the opening of a new channel $s_2 \to s_1 + Z$. The right panel (b) gives the parameter space of m_2 and λ_{22} for the relic abundance. And the solid and dashed lines are numerical results and MadDM's results respectively.

the neutral current J^μ_Z, electromagnetic current $J^\mu_{\rm em}$ and dark current J^μ_D. Z boson also couples to the dark current J^μ_D due to the mixing. All of these interactions are suppressed by ϵ. Specifically, the interactions between mass eigenstate gauge bosons and currents are given in the following at leading order $\mathcal{O}(\epsilon)$,

$$\mathcal{L}_{\rm int} = A_\mu e J^\mu_{\rm em} + Z_\mu \left(g J^\mu_Z - \epsilon g_D \frac{m_Z^2 t_w}{m_Z^2 - m_{A'}^2} J^\mu_D \right) + A'_\mu \left(g_D J^\mu_D + e\epsilon J^\mu_{\rm em} + \epsilon g \frac{m_{A'}^2 t_w}{m_Z^2 - m_{A'}^2} J^\mu_Z \right), \tag{2.18}$$

where J_D is the dark current for complex scalar S,

$$J^\mu_D = i \left(S^\dagger \partial^\mu S - S \partial^\mu S^\dagger \right) = s_2 \partial^\mu s_1 - s_1 \partial^\mu s_2, \tag{2.19}$$

which is invariant under global $\mathrm{U}(1)_D$ rotation.

Moreover, A' does not induce annihilation for σ_{11} and σ_{22}. It only leads to the coannihilation of σ_{12} and the decay of s_2 as $s_2 \to s_1 f\bar{f}$. Both A' and Z can mediate the decay $s_2 \to s_1 f\bar{f}$, but the contribution from Z boson involving J_Z has an extra suppression factor of $(m_1\Delta)^2/m_Z^2$ or $(m_1\Delta)^2/m_{A'}^2$ comparing to the other contributions. This is because the Z boson contribution will be almost canceled by the negative contribution from A' when momentum transfer is small, e.g. $m_1\Delta \ll m_Z,\ m_{A'}$ [57]. As a result, the dominant contribution comes from the amplitude $\epsilon e g_D J^\mu_{\rm em} J_{D,\mu}/m_{A'}^2$ for heavy A' mass. In this case,

JHEP04(2022)024

the decay width of s_2 can be approximately written as

$$\Gamma(s_2 \to s_1 f \bar{f}) \simeq Q_f^2 \frac{(\epsilon g_D)^2 e^2 m_2^5 \Delta^5}{60\pi^3 m_{A'}^4} \simeq Q_f^2 \left(\frac{\epsilon g_D}{10^{-3}}\right)^2 \left(\frac{\Delta}{0.1}\right)^5 \left(\frac{3m_2}{m_{A'}}\right)^4 \frac{m_2}{100\ \text{GeV}} \cdot 0.92\ \text{ns}^{-1}, \tag{2.20}$$

where Q_f is the electric charge of f and $m_{A'}, m_2 \gg m_f$. For the exact calculation and the plots, we use the numerical results from MadGraph for the final state phase space.

We show our approximate results and compare them to the MadGraph results in the left panel of figure 1. In this plot, we choose $m_{A'} = 3m_2$ and $\Delta = 0.05, 0.10, 0.15$ as benchmark points. The decay width of s_2 increases with m_2, as shown in eq. (2.20). Our approximate calculation and MadGraph results are consistent with each other when $m_1\Delta \ll m_Z$. After $m_1\Delta \gtrsim m_Z$, there will be a new decay channel $s_2 \to s_1 Z$, leading to a significant increase of the decay width in the MadGraph results. Moreover, the cancellation of J_Z contribution between Z and A' diagrams is not true anymore. For $\Delta = 0.15$, this new channel opens around 600 GeV, which is shown as the dark red line in the left panel of figure 1; while for $\Delta = 0.10$, this happens around 900 GeV, which is outside of the plot range. For a long-lived s_2 with a decay length around 10 cm, the coupling ϵg_D will be around 25 (4) $\times 10^{-4}$ for $m_2 = 300$ GeV and $\Delta = 0.05(0.10)$. In the right panel of figure 1, the parameter space of m_2 and λ_{22} for the relic abundance are shown. The relic abundance is obtained with the help of coannihilating processes $s_2 s_2 \to$ SM SM. The corresponding $\lambda_{22}(m_2)$ will be used when generating the processes at LHC.

Lastly, there are four point vertex from $\mathcal{L}_{\text{eff}}$ in eq. (2.15), which is an exclusive feature for U(1)$_D$ charged scalar DM models,

$$\frac{g_D^2}{2}(s_1^2 + s_2^2)\left(A'_\mu + \epsilon \frac{m_Z^2 t_w}{m_Z^2 - m_{A'}^2} Z_\mu\right)^2. \tag{2.21}$$

This term is again invariant under global U(1)$_D$ rotation, which will induces pair annihilation into $A'A', A'Z, ZZ$ gauge boson pair. In this work, we will set $m_{A'} = 3m_2$, that the only possible annihilation processes allowed by kinematics are $s_1 s_1 (s_2 s_2) \to ZZ$. However, such processes are suppressed by high power of ϵg_D and the mass ratio $m_Z^2/m_{A'}^2$, which in total is $\mathcal{O}((\epsilon g_D m_Z/m_{A'})^4)$. Thus all the annihilation contributions from the four point interactions to $\sigma_{11,\ 22}$ can be neglected.

3 Existing constraints

We will explore the potential of searching long-lived s_2 at the LHC experiments. In this model, the DM obtains its right relic abundance dominantly through the coannihilation via the quartic interaction $\lambda_{22} s_2 s_2 H^\dagger H$. Therefore, the coupling λ_{22} is sizable and we need to check the existing constraints from collider, direct and indirect experiments. Besides that, there are two more parameters m_2 and Δ. For the coannihilation mechanism, the mass splitting Δ should not be too large and we take 0.05, 0.10 and 0.15 as our benchmark points. For the mass parameter, we take it to be at electroweak scale and pay special attention for large mass > 100 GeV.

JHEP04(2022)024

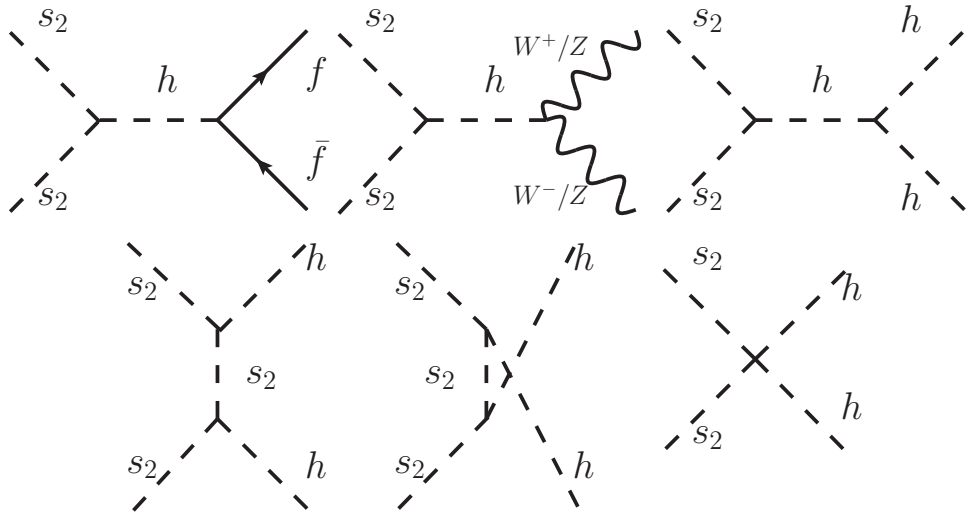

Figure 2. The Feynman diagrams for the annihilation $s_2 s_2 \to$ SM SM.

Relic abundance. For pure-scalar and scalar-vector models, the excited state s_2 couples to SM Higgs via the quartic interaction $\lambda_{22} s_2 s_2 H^\dagger H$, which will lead to pair annihilation cross section for $s_2 s_2 \to$ SM SM. Since the annihilation cross sections σ_{11} and σ_{12} are negligible, the effective cross section $\sigma_{\rm eff}$ is purely determined by λ_{22} once the mass parameters are fixed.

The annihilation processes for $s_2 s_2 \to$ SM SM include the final states $\bar{f}f$, W^+W^-, ZZ and hh, subjected to the kinematic constraints. The corresponding Feynman diagrams are given in figure 2. The s-wave part of the cross sections $\langle \sigma v \rangle_s$ are given below,

$$\langle \sigma v \rangle_s = \langle \sigma v \rangle_{f\bar{f}} + \langle \sigma v \rangle_{WW} + \langle \sigma v \rangle_{ZZ} + \langle \sigma v \rangle_{hh}, \tag{3.1}$$

$$\langle \sigma v \rangle_{f\bar{f}} = \frac{\lambda_{22}^2 m_f^2 (m_2^2 - m_f^2)^{3/2}}{4\pi m_2^3 (4m_2^2 - m_h^2)^2}, \tag{3.2}$$

$$\langle \sigma v \rangle_{WW} = \frac{\lambda_{22}^2 (4m_2^2 - 4m_W^2 m_2^2 + 3m_W^4)\sqrt{m_2^2 - m_W^2}}{8\pi m_2^3 (4m_2^2 - m_h^2)^2}, \tag{3.3}$$

$$\langle \sigma v \rangle_{ZZ} = \frac{\lambda_{22}^2 (4m_2^2 - 4m_Z^2 m_2^2 + 3m_Z^4)\sqrt{m_2^2 - m_Z^2}}{16\pi m_2^3 (4m_2^2 - m_h^2)^2}, \tag{3.4}$$

$$\langle \sigma v \rangle_{hh} = \frac{\lambda_{22}^2 (\lambda_{22} v_h^2 (4m_2^2 - m_h^2) - 4m_2^4 + m_h^4)^2 \sqrt{m_2^2 - m_h^2}}{16\pi m_2^3 \left(8m_2^4 - 6m_2^2 m_h^2 + m_h^4\right)^2}. \tag{3.5}$$

All of the annihilation cross sections are proportional to λ_{22}^2. And the freeze-out temperature is determined by [2, 15, 56]

$$x_f = \ln \frac{0.038 g_{\rm eff} m_{\rm Pl} m_1 \langle \sigma_{\rm eff} v \rangle}{g_*^{1/2} x_f^{1/2}}. \tag{3.6}$$

JHEP04(2022)024

And the relic abundance is

$$\Omega h^2 = \frac{1.07 \times 10^9}{g_*^{1/2} J(x_f) m_{\rm Pl}(\rm GeV)}, \tag{3.7}$$

where $J(x_f) = \int_{x_f}^{\infty} \frac{\langle \sigma_{\rm eff} v \rangle}{x^2} dx$. Together with eq. (2.2), eq. (3.6) and eq. (3.7), we can use numerical iteration to solve the freeze-out temperature x_f and the coupling λ_{22}, which satisfies the DM relic abundance requirement. What's more, we find that the s-wave expansion of annihilation cross-section with small velocity might be invalid near the resonance region ($m_2 \sim m_h/2$), because there exists another small quantity $(4m_2^2 - m_h^2)/m_2^2$. As a result, in order to avoid this effect, we consider its exact thermal average for $m_2 < 80$GeV.

Besides, we also compare it to MadDM [59] in the right panel of figure 1. We can clearly see the analytic results are in agreement with MadDM's in the mass range $[100, 700]$ GeV for $\Delta = 0.05$ and 0.10. While for $\Delta = 0.15$ the MadDM's result is above numerical one, which shows the shortcomings of s-wave approximation. In order to understand the physics, we show the mass range from 10 GeV to 1000 GeV and $\Delta = 0.05,\ 0.10,\ 0.15$ respectively. It shows that the required λ_{22} increases with Δ in general, due to the Boltzmann suppression factor $e^{-2x\Delta}$. For light s_2 mass, e.g. $m_2 < m_h/2$, the required λ_{22} is still larger than heavy m_2 region, because the opening channels are $f\bar{f}$ only which cross sections are suppressed by the small Yukawa couplings. There are dips around $m_2 \sim m_h/2$ due to the SM Higgs resonance. The step features in the plot for large m_2 are originated from the opening of channels, W^+W^-, ZZ, hh and $t\bar{t}$ respectively. Besides, as shown in figure 1(b), for $\Delta = 0.15$ when $m_2 \gtrsim 500$GeV, the yukawa coupling λ_{22} will exceed 4π which violates the perturbation condition, so the red dashed lines in figure 5 indicate this constraint.

In addition to the annihilation via the quartic interaction $\lambda_{22} s_2 s_2 H^\dagger H$, there are more annihilation channels for pure-scalar and scalar-vector model specifically. For the pure-scalar case, there are also contributions from $s_1 s_2 \to h/s_2 \to \text{SM} + \text{SM}$ and $s_2 s_2 \to s_1 \to \text{SM} + \text{SM}$. However, these coannihilation cross sections are proportional to λ_{12}^2, which is tiny comparing to λ_{22}^2. Therefore we can safely ignore those contributions. For the scalar-vector model, there could be contributions from s-channel $s_1 s_2 \to A'/Z \to \text{SM} + \text{SM}$ and t channel $s_2 s_2/(s_1 s_1) \to ZZ/(A'A')$, $s_1 s_2 \to hZ/A'$. The coannihilation cross sections of these processes are proportional to $\epsilon^2 g_D^2$, which is much smaller than λ_{22}^2. At the same time, dark photon mass $m_{A'}$ is set to be $m_{A'} = 3m_2$ to avoid annihilations to on-shell A'. Thus we can ignore all these contributions to the relic abundance.

Thermalization. The calculations above assume the equilibrium between s_1 and s_2 is achieved until freeze-out. The dominate relevant processes are up-scattering (down-scattering) with SM fermions, $s_1 + f \to s_2 + f$. To achieve the equilibrium, we require $\Gamma > H$, where the rate Γ defined as

$$\Gamma(T) = \sum_f n_f^{\rm eq} \langle \sigma_f v \rangle \gtrsim H, \tag{3.8}$$

where σ_f is the scattering cross section. The requirement can easily be satisfied at high temperature, but around freeze out, it require $\epsilon g_D \gtrsim 10^{-4}$. This constraint is shown in figure 5, where it cuts into the lower part of the LLP signal region.

JHEP04(2022)024

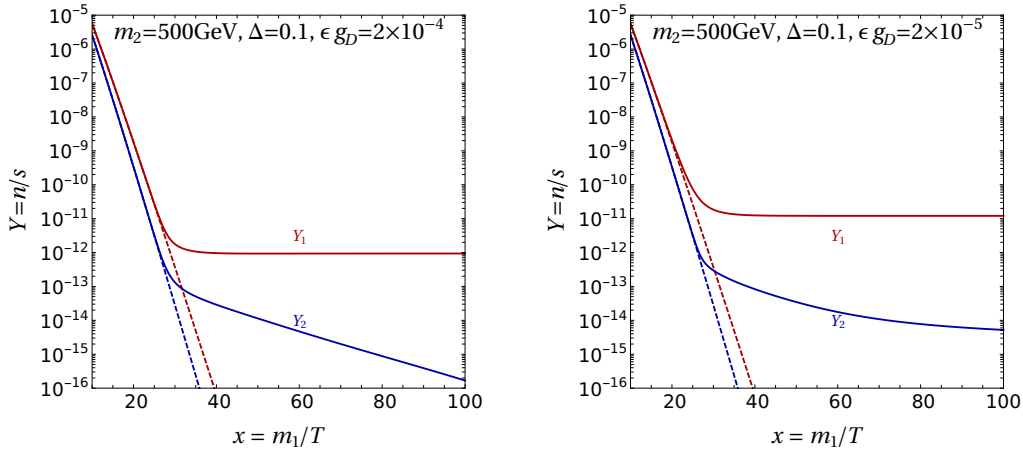

Figure 3. The solutions of coupled Boltzmann equations for two benchmark points. The left panel is for $m_2 = 500\text{GeV},\ \Delta = 0.10,\ \epsilon g_D = 2 \times 10^{-4}$ while the right panel is for $m_2 = 500\text{GeV},\ \Delta = 0.10,\ \epsilon g_D = 2 \times 10^{-5}$.

Moreover, one can make a more careful treatment by solving the coupled Boltzmann equations, which is valid no matter the equilibrium maintained until freeze out or not. The equations are

$$\begin{cases} \dfrac{dY_1}{dx} = -\dfrac{\lambda_f}{x^2} Y_f \left(Y_1 - \dfrac{Y_1^{\rm eq}}{Y_2^{\rm eq}} Y_2 \right) + \gamma x \left(Y_2 - \dfrac{Y_2^{\rm eq}}{Y_1^{\rm eq}} Y_1 \right), \\ \dfrac{dY_2}{dx} = -\dfrac{\lambda_{22}}{x^2} (Y_2^2 - Y_2^{\rm eq2}) + \dfrac{\lambda_f}{x^2} Y_f \left(Y_1 - \dfrac{Y_1^{\rm eq}}{Y_2^{\rm eq}} Y_2 \right) - \gamma x \left(Y_2 - \dfrac{Y_2^{\rm eq}}{Y_1^{\rm eq}} Y_1 \right), \end{cases} \tag{3.9}$$

where $\lambda = \frac{s(m_1)}{H(m_1)} \langle \sigma v \rangle$, $\gamma = \frac{\langle \Gamma_2 \rangle}{H(m_1)}$, and λ_f is for up and down-scattering between the s_1 and s_2 while λ_{22} is for s_2 annihilation into SM particles.

We have tested several benchmarks in our parameters and found that the results are in good agreement with our estimation using eq. (3.8). In figure 3, we numerically solve the coupled Boltzmann equation and show the evolutions for the yield of $s_{1,2}$. We give two benchmark points with ϵg_D above and below the thermalization estimation for $m_2 = 500\text{GeV},\ \Delta = 0.1$. In the case of $\epsilon g_D = 2 \times 10^{-4}$, we find it can satisfy the DM relic abundance $\Omega h^2 = 0.117$. However, in the other case of $\epsilon g_D = 2 \times 10^{-5}$, we find that DM relic abundance is too large, $\Omega h^2 = 1.509$, because DM freeze-out happens too early.

Indirect detection. In our model, the only significant annihilation to SM particles are from $s_2 + s_2$. However, the life-time of s_2 is quite short comparing with the Hubble, thus s_2 already decays before CMB. Therefore, it does not inject energy to the thermal plasma during CMB era or after. While for s_1, it can have the annihilation channel $s_1 s_1 \to hh$ via t-channel s_2, but is suppressed by small $\lambda_{12}^2 \sim 10^{-6}$ if requiring $c\tau_{s_2} \sim 10$ cm. For the vector-scalar case, there could be annihilation channel $s_1 s_1 \to ZZ$ via t-channel s_2 or four point vertex in eq. (2.21), but is suppressed by ϵ^2. Therefore, due to the absence of s_2 in the late universe and the small annihilation cross section of $s_1 s_1$, the indirect detection constraints can not restrain the scalar iDM model.

JHEP04(2022)024

Direct detection. The DM s_1 does not couple to SM particles directly, so the tree-level contribution in dark matter-nucleus/electron elastic scattering is missing. It is a result from the condition $\sigma_{11} \simeq 0$. When going to the full models with s_2 decay, the direct detection cross section should be considered with the presence of s_2. In the pure-scalar case, the coupling λ_{12} will induce loop-level scattering cross section [52]. The spin independent direct detection cross section will be suppressed by $\lambda_{12}^4/(16\pi^2)^2$, which is too small to be constrained. On the other hand, there could be inelastic scattering process for direct detection $s_1 N \to s_2 N$ induced by λ_{12}. But our typical mass difference is $m_1 \cdot \Delta > 1\,\text{GeV}$, which is significantly much larger than the kinetic energy of non-relativistic s_1. Thus, the inelastic scattering is forbidden by the kinematics. For scalar-vector model, there are 1-loop diagram contributions for elastic scattering, via a box diagram mediated by s_2 and a triangle diagram from eq. (2.21) which is special for scalar DM. Such contributions are proportional to ϵ^4 and further suppressed by high powers of $m_Z^2/m_{A'}^2$ and loop factors, thus direct detection experiments does not constrain our parameter space [26, 27].

LHC and electroweak precision test. The coannihilation mechanism requires a large coupling to SM particles, which is realized by the quartic scalar coupling λ_{22}. Through this interaction, the LHC can produce s_2 pair through the Higgs mediated process $pp \to s_2 s_2$, followed by the s_2 decay $s_2 \to s_1 f \bar{f}$. Since the mass difference between s_2 and s_1 is about $\sim 10\%$, the fermions in the final states are quite soft to detect. However, with an extra energetic initial radiation jet, the process $pp \to j + s_2 s_2$ has the same feature as the mono-jet plus missing energy. Therefore, it can be constrained by mono-jet searches at LHC [60, 61]. Our signal cross section without cut is less than 100 fb after fixing λ_{22} by the relic abundance, for $m_2 \in [70, 700]\,\text{GeV}$. The LHC constraint on the cross section is $\sigma A \epsilon < 736\,\text{fb}$ with some basic cuts on p_T and $\not{E}_T$ and acceptance efficiency included, therefore the model we consider is safe from the mono-jet searches.

For the scalar-vector model, there are additional constraints because the dark photon A' couples to the electromagnetic current with the coupling strength ϵe. One important constraint comes from the dilepton resonance search [62, 63], which sets limit on $\sigma(pp \to A')\text{BR}(A' \to \ell^+\ell^-)$. Such cross section is proportional to ϵ^2, however the branching ratio $\text{BR}(A' \to \ell^+\ell^-)$ depends on both ϵ and g_D due to the DM decay channel $A' \to s_1 s_2$. In this study, we fix $m_{A'} = 3m_2$ and in figure 5 we choose $g_D = 0.1$ as a benchmark point. In this case, $\lambda_{22} \gg g_D, \epsilon$, so that the coannihilation are dominated by $s_2 s_2 \to \text{SM SM}$ and the other coannihillation processes are suppressed by small g_D or ϵ. We find that the constraint from dilepton searches at LHC requires $\epsilon \lesssim 0.03$–0.1 for $m_{A'} \in [100,\ 600]\,\text{GeV}$ respectively, as shown in gray shaded region in figure 5. Another relevant constraint for scalar-vector model comes from the electroweak precision test (EWPT) [64], because the mixing between the dark photon and the Z gauge boson. The kinematic mixing from A' can shift Z boson mass and its couplings to SM fermions, thus affects the global fitting of the electroweak observable. For our setup, the EWPT constraint is weaker than the dilepton resonance searches. We plot the relevant constraints in figure 5, which are complementary to the sensitive region from the LLP searches.

JHEP04(2022)024

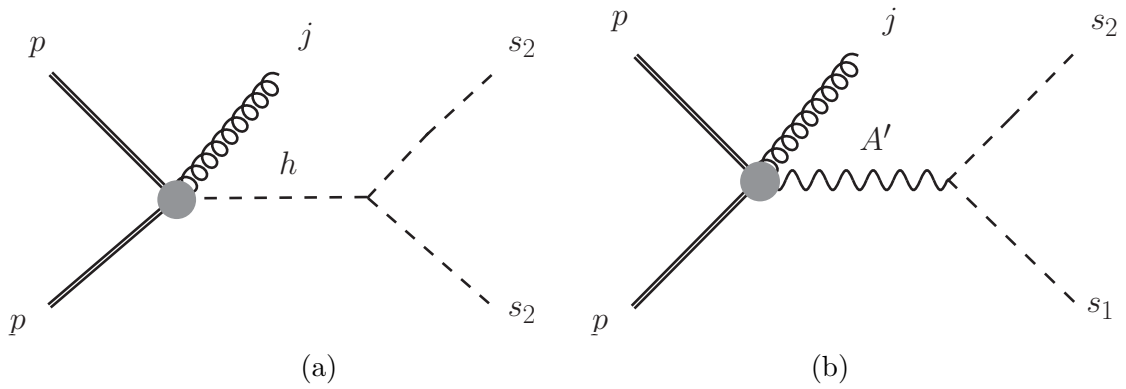

Figure 4. The Feynman diagrams for LHC productions of s_2 in the scalar-vector model.

4 Long-lived particle signatures of the excited dark matter particle

4.1 The production and decay of the long-lived particle

We are interested in the dark sector particles with mass $m_{1,2} \gtrsim \mathcal{O}(100)$GeV, therefore LHC is the most appropriate experiment to look for it. In this section, we discuss the probes of coannihilating DM and its partner at the future high-luminosity LHC (HL-LHC), with the integrated luminosity $\mathcal{L} = 3$ ab^{-1}. For the pure-scalar and scalar-vector models, one can produce the excited states s_2 through Higgs portal or dark photon with an initial state radiation jet, namely

$$pp \to jh^* \to js_2s_2, \quad pp \to jA' \to js_2s_1. \tag{4.1}$$

The Feynman diagrams are listed in figure 4.

The s_2s_2 is produced via s-channel off-shell SM Higgs in both two models, while the s_2s_1 production on the right of eq. (4.1) is specific to the scalar-vector model for heavy $s_{1,2}$, because the A' is heavy enough to decay to s_2s_1 but SM Higgs can not decay to s_2s_1. The first process cross section is only determined by the s_2 mass after fix λ_{22} via the dark matter relic abundance. While for the second process, the cross section depends on ϵ and g_D together with the m_2, even after we fix A' mass as $m_{A'} = 3m_2$. In our study, we focus on the case $\lambda_{22} \gg \epsilon, g_D$, therefore the first one will be the dominant process to search at HL-LHC. As a coannihilation partner, s_2 is unstable and subsequently decays to s_1 and SM particles as

$$s_2 \to s_1 + jj, \quad s_2 \to s_1 + \ell^+\ell^-. \tag{4.2}$$

The former one happens for both pure-scalar and scalar-vector models, and the second one can have a significant branching ratio for scalar-vector model only because of the small lepton mass suppression in Yukawa coupling in pure-scalar model. The leptons are much easier to search at LHC comparing to jets, especially for soft objects. As a result, in this study we will focus on the scalar-vector model and the leptonic decay $s_2 \to s_1 + \ell^+\ell^-$.

4.2 The generic features of the LLPs

For the neutral LLP s_2, its decay can be spatially displaced and also time delayed, depending on its mass and mass splitting. Inside the detector, the decay products of s_2 can be

JHEP04(2022)024

reconstructed as a displaced vertex, which is spatially separated from the interaction point. Therefore, it is different from most of the SM backgrounds which are prompt and can be used to suppress the SM background. Regarding the time delay, it comes from the slow movement of the heavy s_2, which results a time delayed arrival at the detectors. In the future upgrade of the HL-LHC, the timing layers are deployed to suppress the pile-up events and more precise measurements for location, momentum and energy of the particles. For example, CMS is working on the minimum ionizing particle (MIP) timing detector [65, 66], ATLAS is working on the High Granularity Timing Detector [67] and LHCb has the similar precision timing upgrades in the future [68]. For SM particles, especially the mesons and leptons, they are moving at the speed of light. The heavier objects in the SM decay instantly into the light particles, therefore they also have no time lag and their signals arrive at the detector very fast. As a result, the heavy s_2 can significantly lag behind the SM process in time. A quantitative description of the time difference is given as [69]

$$\Delta t_f = L_{s_2}/\beta_{s_2} + L_f/\beta_f - L_{\rm SM}/\beta_{\rm SM}, \tag{4.3}$$

for the decay $s_2 \to s_1 + \bar{f}f$, where β and L denotes the velocity and the moving distance of each particle, and SM denotes a trajectory connecting interaction point and the arrival point at the detector via a SM particle. For simplicity, the trajectories of s_2 and decay products are assumed to be straight lines, and $\beta_f \simeq \beta_{\rm SM} \simeq 1$ are adopted. For b quark or τ lepton, they are heavy but decay fairly quickly into light leptons, mesons or hadrons, which are again ultra-relativistic. Therefore, the above assumptions are viable.

Regarding the signal trigger, we always require an initial state radiation jet accompanied with the signal, which can time stamp the primary vertex [69]. A hard initial state radiation jet with $p_T^j > 120\,\text{GeV}$ can also trigger the signal event with Jet+MET tagger [70, 71]. There are other triggers which can help loosen the requirements on the hard leading jet. For example, people have discussed using the displaced track information to implement the L1 hardware trigger, and the requirement on the track p_T can be as low as 2 GeV [72–79]. The delayed photon and jet are studied in refs. [69, 80, 81] to set limits for LLPs. Using delayed objects for trigger is under discussion and development [65]. In the ATLAS experiment, one can also use the Muon Spectrometer Region of Interest method to trigger the displaced events [82]. In summary, there are many ways to improve the triggers for the LLP signal. As a result, a trigger with a hard initial jet radiation is quite conservative and could be further improved. With the presence of leptons, the trigger becomes even more easier comparing with pure hadronic final states. The specific triggers, signal cuts and the background estimates will be addressed in the later subsections.

Besides the ATLAS and CMS experiments, there are also dedicated experiments or future plans for LLPs, such as MATHUSLA (MAssive Timing Hodoscope for Ultra-Stable neutraL pArticles) [83, 84], FASER [85, 86], CODEX-b [87]. We consider all of them and find that the MATHUSLA experiment is much better than FASER and CODEX-b due to the specific model and the parameter space we are interested in. We stress that the work will focus on the scalar-vector model in the LLP study. The signature of pure-scalar model includes soft jets, which trigger and QCD background are very challenging. Some track based strategies may reduced background [88, 89], but we will leave it for the future work.

JHEP04(2022)024

4.3 The scalar-vector model at LHC

In the scalar-vector model, there are two production channels for s_2, which are shown in figure 4. The left panel is realized via off-shell Higgs boson, and the right panel is realized via on-shell A'. As shown in the right panel of figure 1, one needs $\lambda_{22} \sim \mathcal{O}(1)$ to realize the right dark matter relic abundance. Since the ϵ and g_D are much smaller than λ_{22}, the main production channel of s_2 in LHC is by exchanging off-shell Higgs and its cross section is proportional to λ_{22}^2. The other production channel $pp \to jA'$ is proportional to ϵ^2. When ϵ is large enough, the on-shell production of A', followed by $A' \to s_1 s_2$ decay is considered in our calculation. In this work, we fix $g_D = 0.1$ and $m_{A'} = 3m_2$ as our benchmark point to reduce the parameters.

The excited state s_2 couples to s_1 mainly through dark photon A'. Since we assume heavy A', then s_2 will only decay to $s_1 f \bar{f}$ via off-shell A'. Because A' couples to all the SM electromagnetic current via the kinetic mixing, for a reasonable consideration we can have $2m_b < m_1 \cdot \Delta < 2m_t$, with b, t denoting bottom and top quarks. The total width of s_2 is

$$\Gamma_{s_2} \simeq \frac{(\epsilon g_D e)^2 m_2^5 \Delta^5}{9\pi^3 m_{A'}^4}, \tag{4.4}$$

which is shown in the left panel of figure 1. The signals we consider for scalar-vector model are

$$pp \to j s_2 s_2 \ (j s_2 s_1), \quad s_2 \to s_1 \ell^+ \ell^-. \tag{4.5}$$

We take the inclusive strategy that at least one of s_2 decays to leptons in the detector. The branching ratio of $s_2 \to s_1 \ \ell^+ \ \ell^-$ can be estimated as 3/10 by counting the degrees of freedom of the particles, where $\ell = e, \ \mu$. Another important physical parameter is the lifetime of s_2, $\tau = 1/\Gamma$, for the LLP searches at HL-LHC. The last important free parameter is the mass difference Δ, which is important for triggering the signal via the leptons. In summary, there are only three free physical parameters, after we assume $g_D = 0.1$, $m_{A'} = 3m_2$ and fix λ_{22} by relic abundance, which are

$$\{m_2, \Delta, \epsilon\}\,. \tag{4.6}$$

There are many strategies to look for LLPs together with different triggers [90]. Since the s_2's decay products contain leptons, it is easier to trigger. For example, in CMS Run-2, the scouting technique has been used to select two muons events with p_T as low as 3 GeV [90]. One search strategy relies on the presence of displaced muons, denoted as *displaced muon-jet* (DMJ) [26], and worked conservatively with the Jet+MET trigger [70, 71]. Therefore, the detailed cuts are [26, 27],

$$\text{DMJ}: \ p_T^j > 120 \text{ GeV}, \quad p_T^\mu > 5 \text{ GeV}, \quad r_{s_2} < 30 \text{ cm}, \quad d_0^\mu > 1 \text{ mm}, \tag{4.7}$$

where r_{s_2} is a radial displacement of the s_2 decay vertex and d_0 is transverse impact parameter. The condition $r_{s_2} < 30$ cm guarantees the s_2 decay leaves tracks in the tracking system. The backgrounds can be reduced to a negligible level after the above cuts [26].

JHEP04(2022)024

Another possible strategy utilizes the time delay of heavy LLP, and the leptons are not specified to muons [27]. Specifically, the cuts are taken as

$$\begin{aligned} \text{Timing}: \quad & p_T^j > 120 \text{ GeV } (30 \text{ GeV}), \quad p_T^\ell > 3 \text{ GeV}, \quad |\eta| < 2.4, \\ & \Delta t_\ell > 0.3 \text{ ns}, \quad 5 \text{ cm} < r_{s_2} < 1.17 \text{ m}, \quad z_{s_2} < 3.04 \text{ m}, \end{aligned} \tag{4.8}$$

where η is the pseudo-rapidity for the jet and leptons. The time delay for leptons Δt_ℓ are used to suppress the SM background. The radius and longitudinal location of the decay vertex, r_{s_2} and z_{s_2}, have to be within the CMS MIP timing detector to ensure the hits on the timing layer. For the initial state radiation, the p_T^j cut has two choices. One is conservative, $p_T^j > 120$ GeV, which is used by the conventional Jet+MET trigger. On the other hand, one can also be optimistic with timing information and the presence of the leptons, that a lower threshold $p_T^j > 30$ GeV is possible in the near future. The backgrounds can be sufficiently suppressed with the above cuts, therefore the SM backgrounds are taken to be zero [27, 69].

Aside from LHC detectors, MATHUSLA is a proposed LLP detector at CERN, located on the surface. The main detector is 20 meters tall and 200m $\times$ 200m in area. MATHUSLA is shielded by $\sim$ 100 m of rock to keep out of QCD backgrounds. The bottom and side of MATHUSLA are covered with scintillator to veto incoming charged particles, such as high energy muons and cosmic rays. In conclusion, the LLP search at MATHUSLA can be assumed to be background free. In order to consider the sensitivity on s_2 search at MATHUSLA, we require s_2 to decay inside its decay volume,

$$\text{MATHUSLA}: 100 \text{ m} < x_{s_2} < 120\text{m}, -100\text{m} < y_{s_2} < 100\text{m}, 100 \text{ m} < z_{s_2} < 300\text{m}. \tag{4.9}$$

One considers the signals as charged tracks with energy deposition of more than 600 MeV, following the discussion in ref. [84].

The signal event number for s_2 decay that satisfying the selection criteria can be expressed as

$$N_{\text{sig}}^{\ell\ell} = \mathcal{L} \cdot \sigma_{\text{sig}} \cdot P(s_2) \cdot \epsilon_{\text{cut}}, \tag{4.10}$$

where $P(s_2)$ is the s_2 decay possibility inside the decay volume, $\mathcal{L} = 3\text{ab}^{-1}$ is the integrated luminosity and ϵ_{cut} is the total cut efficiency. We use the Monte Carlo simulation to determine the decay time of s_2 according to its momentum direction and lifetime, then fix the location of decay vertex (r_{s_2} and z_{s_2}) and finally calculate the parameters Δt_ℓ according to the kinematics of s_2 and ℓ.

Based on the three cut conditions listed above, we show the sensitivities for three search strategies in figure 5 for $\Delta = 0.05,\ 0.10$ and 0.15, with signal events reaching $N = 2.3$ and 10. We can see that the timing search strategy has better reach for smaller ϵ than DMJ strategy. Because it prefers longer life-time comparing to DMJ method. For the optimistic leading jet p_T cut (dashed cyan), the sensitivities increase significantly comparing with the conservative p_T cut. For the DMJ method, it is subject to the requirement that s_2 decays inside the tracker system, which prefers larger ϵ. At the same time, as stated before, $\sigma(pp \to jA')$ is proportional to ϵ^2, so when fixing $g_D = 0.1$ larger ϵg_D will induce larger cross section of A' resonance. The sensitivity at LHC will cover the region from $\epsilon g_D = 10^{-2}$ to 10^{-4} combing these two strategies for m_2 around 100–500 GeV. For heavier mass, the A' is too

JHEP04(2022)024

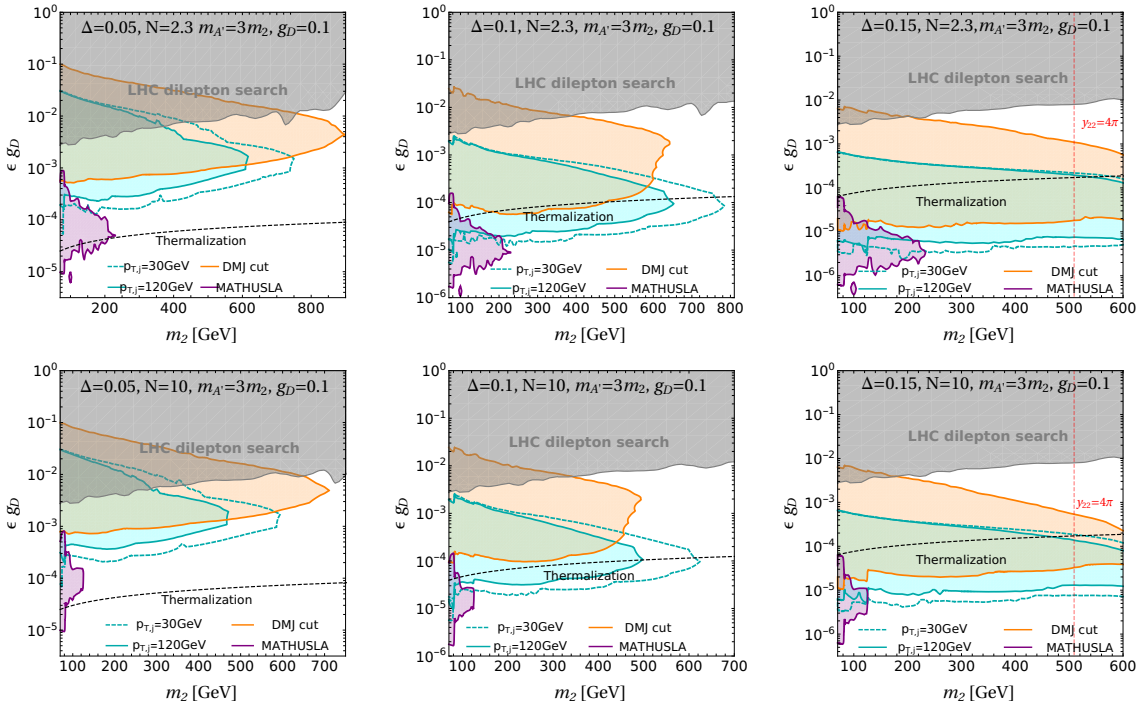

Figure 5. The expected sensitivity at HL-LHC to the scalar-vector model in the ϵg_D, m_2 plane for $\mathcal{L} = 3$ ab^{-1} and $\sqrt{s} = 13$ TeV. We have three panels from left to right for $\Delta = 0.05$, $\Delta = 0.10$ and $\Delta = 0.15$ respectively, and top (bottom) panels for the signal event number $N_{\rm sig}^{\ell\ell} = 2.3$ (10) respectively. The heavy dark photon mass is set as $m_{A'} = 3m_2$ and we assume $g_D = 0.1$. The constraints from LHC dilepton searches are plotted in gray shaded region. For LLPs search, the projected reach for time delay strategy with ISR jet $p_T^j > 120$GeV(30GeV) and are shown as cyan solid (dashed) contours respectively. The orange (purple) contours show the projected reach for DMJ strategy (MATHUSLA detector)respectively. The black dashed contours indicate the thermal equilibrium condition. The red dashed contours show the constraints from the perturbation condition.

heavy to produce on-shell, thus the sensitivities are greatly suppressed. For MUTHUSLA search, it is not as sensitive as the two methods at ATLAS and CMS. It is because the MATHUSLA detector requires longer decay length ~ 100 m and a smaller angular volume. Therefore, s_2 can arrive at the decay volume with a lower possibility, especially for heavy s_2.

In figure 5, there is a dip at $m_2 = m_Z$, because the sudden drop of λ_{22} at $m_2 = m_Z$, which is also the reason for the island in the MATHUSLA search. Moreover, we compare the sensitivities between $\Delta = 0.05$, $\Delta = 0.10$ and $\Delta = 0.15$. The sensitivity for $\Delta = 0.15$ is generally better than the case of $\Delta = 0.05$ and $\Delta = 0.10$ when mass is same, because larger Δ will require larger λ_{22} for the DM relic abundance. Thus, it results in a larger cross section for $pp \to j s_2 s_2$. Furthermore, larger Δ will lead to more energetic decay products from s_2, which helps signal to pass the cut conditions.

It is worth mentioning that when $m_1\Delta \gtrsim m_Z$, there will be $s_2 \to s_1 Z$ decay open with an on-shell Z. Although both suppressed by the factor $\epsilon^2 g_D^2$, it will be more significant in branching ratio comparing with $s_2 \to s_1 \ell^+ \ell^-$, because it is 2-body final state phase-space.

JHEP04(2022)024

It leads to an additional information that the invariant mass of the displaced lepton pair should be around mass of Z, which can help to further suppress the SM background and lower the requirement in the trigger [91]. In our current strategies, the sensitivity region can not reach the region with $m_1\Delta \gtrsim m_Z$. But with less stringent cuts and triggers, it may reach this region, then this invariant mass information can play a role.

5 Conclusions

The coannihilation mechanism of DM can be used to evade the direct detection constraints. Usually, the coannihilation partner needs a sizable coupling to SM particles to obtain a large thermal cross section for the relic abundance. On the other hand, the coannihilation partner can be potentially long-lived at the detector scale, with the small coupling and mass splitting to the DM particle. Previous studies mainly focus on the coannihilation between DM and the coannihilation partner, which limits their mass to be lighter than 100 GeV. In this work, we turn to the case that the coannihilation happens between the partner pair dominantly. This scenario opens heavy mass regions for DM and its coannihilation partner, and we focus on the collider searches for the long-lived coannihilation partner.

We introduced a generic model in which the DM candidate and its coannihilation partner are scalar particles, embedded in the iDM model. With the help of a broken symmetry, only the coannihilation partner couples to SM particles through a special Higgs portal coupling. The coannihilation partner pair annihilation dominates the DM effective annihilation cross section, while the DM-DM and DM-partner annihilation cross sections are negligible. Next, we introduced two specific models to illustrate how coannihilation partner can decay back to the DM particle and be long-lived. The current limits from collider, indirect and direct searches are studied for the scenario and we propose to explore the model via the long-lived coannihilation partner. We considered three methods here, namely displaced muon-jet method, timing method and MATHUSLA searches. The first two methods utilized existing LHC detectors, ATLAS and CMS, together with appropriate triggers for the LLPs. The basic cuts of triggers have been significantly relaxed by the presence of leptons in the partner decay final states. The two methods shows good sensitivities for coannihilation partner with mass smaller than 500 GeV and kinetic mixing parameter ϵ between $10^{-1} - 10^{-4}$ for $g_D = 0.1$. While the MATHUSLA search is less sensitive due to the small lifetime of the partner and the small angular decay volume. In general, the LLP searches can provide a good sensitivity for the coannihilation DM scenario, which is complementary to the generic DM searches and can help to solve the mystery of the DM problem.

Acknowledgments

The work of JL is supported by National Science Foundation of China under Grant No. 12075005 and by Peking University under startup Grant No. 7101502597. The work of XPW is supported by National Science Foundation of China under Grant No. 12005009.

JHEP04(2022)024

References

[1] Planck collaboration, *Planck* 2018 *results. VI. Cosmological parameters*, *Astron. Astrophys.* **641** (2020) A6 [*Erratum ibid.* **652** (2021) C4] [arXiv:1807.06209] [inSPIRE].

[2] K. Griest and D. Seckel, *Three exceptions in the calculation of relic abundances*, *Phys. Rev. D* **43** (1991) 3191 [inSPIRE].

[3] T.R. Slatyer, *Indirect dark matter signatures in the cosmic dark ages. I. Generalizing the bound on s-wave dark matter annihilation from Planck results*, *Phys. Rev. D* **93** (2016) 023527 [arXiv:1506.03811] [inSPIRE].

[4] AMS collaboration, *Electron and positron fluxes in primary cosmic rays measured with the Alpha Magnetic Spectrometer on the International Space Station*, *Phys. Rev. Lett.* **113** (2014) 121102 [inSPIRE].

[5] AMS collaboration, *High statistics measurement of the positron fraction in primary cosmic rays of* 0.5–500 *GeV with the Alpha Magnetic Spectrometer on the International Space Station*, *Phys. Rev. Lett.* **113** (2014) 121101 [inSPIRE].

[6] Fermi-LAT collaboration, *Searching for dark matter annihilation from Milky Way dwarf spheroidal galaxies with six years of Fermi Large Area Telescope data*, *Phys. Rev. Lett.* **115** (2015) 231301 [arXiv:1503.02641] [inSPIRE].

[7] Fermi-LAT and DES collaborations, *Searching for dark matter annihilation in recently discovered Milky Way satellites with Fermi-LAT*, *Astrophys. J.* **834** (2017) 110 [arXiv:1611.03184] [inSPIRE].

[8] DAMPE collaboration, *Direct detection of a break in the teraelectronvolt cosmic-ray spectrum of electrons and positrons*, *Nature* **552** (2017) 63 [arXiv:1711.10981] [inSPIRE].

[9] LUX collaboration, *Results from a search for dark matter in the complete LUX exposure*, *Phys. Rev. Lett.* **118** (2017) 021303 [arXiv:1608.07648] [inSPIRE].

[10] CDEX collaboration, *Constraints on spin-independent nucleus scattering with sub-GeV weakly interacting massive particle dark matter from the CDEX-1B experiment at the China Jinping underground laboratory*, *Phys. Rev. Lett.* **123** (2019) 161301 [arXiv:1905.00354] [inSPIRE].

[11] XENON collaboration, *Dark matter search results from a one ton-year exposure of XENON1T*, *Phys. Rev. Lett.* **121** (2018) 111302 [arXiv:1805.12562] [inSPIRE].

[12] PandaX-4T collaboration, *Dark matter search results from the PandaX-4T commissioning run*, *Phys. Rev. Lett.* **127** (2021) 261802 [arXiv:2107.13438] [inSPIRE].

[13] J. Alimena et al., *Searching for long-lived particles beyond the Standard Model at the Large Hadron Collider*, *J. Phys. G* **47** (2020) 090501 [arXiv:1903.04497] [inSPIRE].

[14] G. Jungman, M. Kamionkowski and K. Griest, *Supersymmetric dark matter*, *Phys. Rept.* **267** (1996) 195 [hep-ph/9506380] [inSPIRE].

[15] J. Edsjo and P. Gondolo, *Neutralino relic density including coannihilations*, *Phys. Rev. D* **56** (1997) 1879 [hep-ph/9704361] [inSPIRE].

JHEP04(2022)024

[16] J.R. Ellis, T. Falk, K.A. Olive and M. Srednicki, *Calculations of neutralino-stau coannihilation channels and the cosmologically relevant region of MSSM parameter space*, *Astropart. Phys.* **13** (2000) 181 [*Erratum ibid.* **15** (2001) 413] [hep-ph/9905481] [INSPIRE].

[17] M.J. Baker et al., *The coannihilation codex*, *JHEP* **12** (2015) 120 [arXiv:1510.03434] [INSPIRE].

[18] G. Bertone and D. Hooper, *History of dark matter*, *Rev. Mod. Phys.* **90** (2018) 045002 [arXiv:1605.04909] [INSPIRE].

[19] M. Buschmann et al., *Hunting for dark matter coannihilation by mixing dijet resonances and missing transverse energy*, *JHEP* **09** (2016) 033 [arXiv:1605.08056] [INSPIRE].

[20] A. Albert et al., *Towards the next generation of simplified dark matter models*, *Phys. Dark Univ.* **16** (2017) 49 [arXiv:1607.06680] [INSPIRE].

[21] O. Buchmueller et al., *Simplified models for displaced dark matter signatures*, *JHEP* **09** (2017) 076 [arXiv:1704.06515] [INSPIRE].

[22] V.V. Khoze, A.D. Plascencia and K. Sakurai, *Simplified models of dark matter with a long-lived co-annihilation partner*, *JHEP* **06** (2017) 041 [arXiv:1702.00750] [INSPIRE].

[23] F. Ambrogi et al., *SModelS v1.2: long-lived particles, combination of signal regions, and other novelties*, *Comput. Phys. Commun.* **251** (2020) 106848 [arXiv:1811.10624] [INSPIRE].

[24] D. Tucker-Smith and N. Weiner, *Inelastic dark matter*, *Phys. Rev. D* **64** (2001) 043502 [hep-ph/0101138] [INSPIRE].

[25] D. Tucker-Smith and N. Weiner, *The status of inelastic dark matter*, *Phys. Rev. D* **72** (2005) 063509 [hep-ph/0402065] [INSPIRE].

[26] E. Izaguirre, G. Krnjaic and B. Shuve, *Discovering inelastic thermal-relic dark matter at colliders*, *Phys. Rev. D* **93** (2016) 063523 [arXiv:1508.03050] [INSPIRE].

[27] A. Berlin and F. Kling, *Inelastic dark matter at the LHC lifetime frontier: ATLAS, CMS, LHCb, CODEX-b, FASER, and MATHUSLA*, *Phys. Rev. D* **99** (2019) 015021 [arXiv:1810.01879] [INSPIRE].

[28] M. Duerr, T. Ferber, C. Garcia-Cely, C. Hearty and K. Schmidt-Hoberg, *Long-lived dark Higgs and inelastic dark matter at Belle II*, *JHEP* **04** (2021) 146 [arXiv:2012.08595] [INSPIRE].

[29] D.W. Kang, P. Ko and C.-T. Lu, *Exploring properties of long-lived particles in inelastic dark matter models at Belle II*, *JHEP* **04** (2021) 269 [arXiv:2101.02503] [INSPIRE].

[30] E. Izaguirre, Y. Kahn, G. Krnjaic and M. Moschella, *Testing light dark matter coannihilation with fixed-target experiments*, *Phys. Rev. D* **96** (2017) 055007 [arXiv:1703.06881] [INSPIRE].

[31] B. Batell, J. Berger, L. Darmé and C. Frugiuele, *Inelastic dark matter at the Fermilab short baseline neutrino program*, *Phys. Rev. D* **104** (2021) 075026 [arXiv:2106.04584] [INSPIRE].

[32] G. Mohlabeng, *Revisiting the dark photon explanation of the muon anomalous magnetic moment*, *Phys. Rev. D* **99** (2019) 115001 [arXiv:1902.05075] [INSPIRE].

[33] Y.-D. Tsai, P. deNiverville and M.X. Liu, *Dark photon and muon $g-2$ inspired inelastic dark matter models at the high-energy intensity frontier*, *Phys. Rev. Lett.* **126** (2021) 181801 [arXiv:1908.07525] [INSPIRE].

[34] V. Silveira and A. Zee, *Scalar phantoms*, *Phys. Lett. B* **161** (1985) 136 [INSPIRE].

JHEP04(2022)024

[35] J. McDonald, *Gauge singlet scalars as cold dark matter*, *Phys. Rev. D* **50** (1994) 3637 [hep-ph/0702143] [INSPIRE].

[36] C.P. Burgess, M. Pospelov and T. ter Veldhuis, *The minimal model of nonbaryonic dark matter: a singlet scalar*, *Nucl. Phys. B* **619** (2001) 709 [hep-ph/0011335] [INSPIRE].

[37] H. Davoudiasl, R. Kitano, T. Li and H. Murayama, *The new minimal Standard Model*, *Phys. Lett. B* **609** (2005) 117 [hep-ph/0405097] [INSPIRE].

[38] V. Barger, P. Langacker, M. McCaskey, M.J. Ramsey-Musolf and G. Shaughnessy, *LHC phenomenology of an extended Standard Model with a real scalar singlet*, *Phys. Rev. D* **77** (2008) 035005 [arXiv:0706.4311] [INSPIRE].

[39] V. Barger, P. Langacker, M. McCaskey, M. Ramsey-Musolf and G. Shaughnessy, *Complex singlet extension of the Standard Model*, *Phys. Rev. D* **79** (2009) 015018 [arXiv:0811.0393] [INSPIRE].

[40] R.N. Lerner and J. McDonald, *Gauge singlet scalar as inflaton and thermal relic dark matter*, *Phys. Rev. D* **80** (2009) 123507 [arXiv:0909.0520] [INSPIRE].

[41] B. Grzadkowski and J. Wudka, *Pragmatic approach to the little hierarchy problem: the case for dark matter and neutrino physics*, *Phys. Rev. Lett.* **103** (2009) 091802 [arXiv:0902.0628] [INSPIRE].

[42] J.M. Cline, K. Kainulainen, P. Scott and C. Weniger, *Update on scalar singlet dark matter*, *Phys. Rev. D* **88** (2013) 055025 [*Erratum ibid.* **92** (2015) 039906] [arXiv:1306.4710] [INSPIRE].

[43] L. Feng, S. Profumo and L. Ubaldi, *Closing in on singlet scalar dark matter: LUX, invisible Higgs decays and gamma-ray lines*, *JHEP* **03** (2015) 045 [arXiv:1412.1105] [INSPIRE].

[44] H. Han and S. Zheng, *Higgs-portal scalar dark matter: scattering cross section and observable limits*, *Nucl. Phys. B* **914** (2017) 248 [arXiv:1510.06165] [INSPIRE].

[45] H. Wu and S. Zheng, *Scalar dark matter: real vs complex*, *JHEP* **03** (2017) 142 [arXiv:1610.06292] [INSPIRE].

[46] M. Escudero, A. Berlin, D. Hooper and M.-X. Lin, *Toward (finally!) ruling out Z and Higgs mediated dark matter models*, *JCAP* **12** (2016) 029 [arXiv:1609.09079] [INSPIRE].

[47] GAMBIT collaboration, *Global analyses of Higgs portal singlet dark matter models using GAMBIT*, *Eur. Phys. J. C* **79** (2019) 38 [arXiv:1808.10465] [INSPIRE].

[48] P. Athron, J.M. Cornell, F. Kahlhoefer, J. McKay, P. Scott and S. Wild, *Impact of vacuum stability, perturbativity and XENON1T on global fits of Z_2 and Z_3 scalar singlet dark matter*, *Eur. Phys. J. C* **78** (2018) 830 [arXiv:1806.11281] [INSPIRE].

[49] PandaX-II collaboration, *Dark matter results from 54-ton-day exposure of PandaX-II experiment*, *Phys. Rev. Lett.* **119** (2017) 181302 [arXiv:1708.06917] [INSPIRE].

[50] PandaX-II collaboration, *Results of dark matter search using the full PandaX-II exposure*, *Chin. Phys. C* **44** (2020) 125001 [arXiv:2007.15469] [INSPIRE].

[51] K. Ghorbani and H. Ghorbani, *Scalar split WIMPs in future direct detection experiments*, *Phys. Rev. D* **93** (2016) 055012 [arXiv:1501.00206] [INSPIRE].

[52] J.A. Casas, D.G. Cerdeño, J.M. Moreno and J. Quilis, *Reopening the Higgs portal for single scalar dark matter*, *JHEP* **05** (2017) 036 [arXiv:1701.08134] [INSPIRE].

JHEP04(2022)024

[53] L. Coito, C. Faubel, J. Herrero-Garcia and A. Santamaria, *Dark matter from a complex scalar singlet: the role of dark CP and other discrete symmetries*, *JHEP* **11** (2021) 202 [arXiv:2106.05289] [INSPIRE].

[54] T.N. Maity and T.S. Ray, *Exchange driven freeze out of dark matter*, *Phys. Rev. D* **101** (2020) 103013 [arXiv:1908.10343] [INSPIRE].

[55] R.T. D'Agnolo, C. Mondino, J.T. Ruderman and P.-J. Wang, *Exponentially light dark matter from coannihilation*, *JHEP* **08** (2018) 079 [arXiv:1803.02901] [INSPIRE].

[56] N.F. Bell, Y. Cai and A.D. Medina, *Co-annihilating dark matter: effective operator analysis and collider phenomenology*, *Phys. Rev. D* **89** (2014) 115001 [arXiv:1311.6169] [INSPIRE].

[57] J. Liu, X.-P. Wang and F. Yu, *A tale of two portals: testing light, hidden new physics at future e^+e^- colliders*, *JHEP* **06** (2017) 077 [arXiv:1704.00730] [INSPIRE].

[58] J. Liu, L.-T. Wang, X.-P. Wang and W. Xue, *Exposing the dark sector with future Z factories*, *Phys. Rev. D* **97** (2018) 095044 [arXiv:1712.07237] [INSPIRE].

[59] F. Ambrogi et al., *MadDM v.3.0: a comprehensive tool for dark matter studies*, *Phys. Dark Univ.* **24** (2019) 100249 [arXiv:1804.00044] [INSPIRE].

[60] ATLAS collaboration, *Search for new phenomena in events with an energetic jet and missing transverse momentum in pp collisions at $\sqrt{s} = 13$ TeV with the ATLAS detector*, *Phys. Rev. D* **103** (2021) 112006 [arXiv:2102.10874] [INSPIRE].

[61] CMS collaboration, *Search for new particles in events with energetic jets and large missing transverse momentum in proton-proton collisions at $\sqrt{s} = 13$ TeV*, *JHEP* **11** (2021) 153 [arXiv:2107.13021] [INSPIRE].

[62] ATLAS collaboration, *Search for high-mass dilepton resonances using 139 fb^{-1} of pp collision data collected at $\sqrt{s} = 13$ TeV with the ATLAS detector*, *Phys. Lett. B* **796** (2019) 68 [arXiv:1903.06248] [INSPIRE].

[63] CMS collaboration, *Search for resonant and nonresonant new phenomena in high-mass dilepton final states at $\sqrt{s} = 13$ TeV*, *JHEP* **07** (2021) 208 [arXiv:2103.02708] [INSPIRE].

[64] D. Curtin, R. Essig, S. Gori and J. Shelton, *Illuminating dark photons with high-energy colliders*, *JHEP* **02** (2015) 157 [arXiv:1412.0018] [INSPIRE].

[65] CMS collaboration, *Technical proposal for a MIP timing detector in the CMS experiment phase 2 upgrade*, Tech. Rep. CERN-LHCC-2017-027, CERN, Geneva, Switzerland (2017).

[66] D. Contardo, M. Klute, J. Mans, L. Silvestris and J. Butler, *Technical proposal for the phase-II upgrade of the CMS detector*, Tech. Rep. CERN-LHCC-2015-010, CERN, Geneva, Switzerland (2015).

[67] C. Allaire et al., *Beam test measurements of low gain avalanche detector single pads and arrays for the ATLAS high granularity timing detector*, 2018 *JINST* **13** P06017 [arXiv:1804.00622] [INSPIRE].

[68] LHCb collaboration, *Physics case for an LHCb upgrade II — opportunities in flavour physics, and beyond, in the HL-LHC era*, arXiv:1808.08865 [INSPIRE].

[69] J. Liu, Z. Liu and L.-T. Wang, *Enhancing long-lived particles searches at the LHC with precision timing information*, *Phys. Rev. Lett.* **122** (2019) 131801 [arXiv:1805.05957] [INSPIRE].

JHEP04(2022)024

[70] CMS collaboration, *Search for dark matter, extra dimensions, and unparticles in monojet events in proton-proton collisions at* $\sqrt{s} = 8$ *TeV*, *Eur. Phys. J. C* **75** (2015) 235 [arXiv:1408.3583] [INSPIRE].

[71] CMS collaboration, *Performance of missing transverse momentum reconstruction in proton-proton collisions at* $\sqrt{s} = 13$ *TeV using the CMS detector*, 2019 *JINST* **14** P07004 [arXiv:1903.06078] [INSPIRE].

[72] E. Bartz et al., *FPGA-based tracklet approach to level-1 track finding at CMS for the HL-LHC*, *EPJ Web Conf.* **150** (2017) 00016 [arXiv:1706.09225] [INSPIRE].

[73] I. Tomalin et al., *An FPGA based track finder for the L1 trigger of the CMS experiment at the High Luminosity LHC*, 2017 *JINST* **12** P12019 [INSPIRE].

[74] CMS collaboration, *First level track jet trigger for displaced jets at High Luminosity LHC*, Tech. Rep. CMS-PAS-FTR-18-018, CERN, Geneva, Switzerland (2018).

[75] Y. Gershtein, *CMS hardware track trigger: new opportunities for long-lived particle searches at the HL-LHC*, *Phys. Rev. D* **96** (2017) 035027 [arXiv:1705.04321] [INSPIRE].

[76] M. Mårtensson, M. Isacson, H. Hahne, R. Gonzalez Suarez and R. Brenner, *To catch a long-lived particle: hit selection towards a regional hardware track trigger implementation*, 2019 *JINST* **14** P11009 [arXiv:1907.09846] [INSPIRE].

[77] Y. Gershtein and S. Knapen, *Trigger strategy for displaced muon pairs following the CMS phase II upgrades*, *Phys. Rev. D* **101** (2020) 032003 [arXiv:1907.00007] [INSPIRE].

[78] A. Ryd and L. Skinnari, *Tracking triggers for the HL-LHC*, *Ann. Rev. Nucl. Part. Sci.* **70** (2020) 171 [arXiv:2010.13557] [INSPIRE].

[79] Y. Gershtein, S. Knapen and D. Redigolo, *Probing naturally light singlets with a displaced vertex trigger*, *Phys. Lett. B* **823** (2021) 136758 [arXiv:2012.07864] [INSPIRE].

[80] ATLAS collaboration, *Search for nonpointing and delayed photons in the diphoton and missing transverse momentum final state in 8 TeV pp collisions at the LHC using the ATLAS detector*, *Phys. Rev. D* **90** (2014) 112005 [arXiv:1409.5542] [INSPIRE].

[81] CMS collaboration, *Search for long-lived particles using nonprompt jets and missing transverse momentum with proton-proton collisions at* $\sqrt{s} = 13$ *TeV*, *Phys. Lett. B* **797** (2019) 134876 [arXiv:1906.06441] [INSPIRE].

[82] ATLAS collaboration, *Search for long-lived, weakly interacting particles that decay to displaced hadronic jets in proton-proton collisions at* $\sqrt{s} = 8$ *TeV with the ATLAS detector*, *Phys. Rev. D* **92** (2015) 012010 [arXiv:1504.03634] [INSPIRE].

[83] J.P. Chou, D. Curtin and H.J. Lubatti, *New detectors to explore the lifetime frontier*, *Phys. Lett. B* **767** (2017) 29 [arXiv:1606.06298] [INSPIRE].

[84] D. Curtin et al., *Long-lived particles at the energy frontier: the MATHUSLA physics case*, *Rept. Prog. Phys.* **82** (2019) 116201 [arXiv:1806.07396] [INSPIRE].

[85] F. Kling and S. Trojanowski, *Heavy neutral leptons at FASER*, *Phys. Rev. D* **97** (2018) 095016 [arXiv:1801.08947] [INSPIRE].

[86] J.L. Feng, I. Galon, F. Kling and S. Trojanowski, *ForwArd Search ExpeRiment at the LHC*, *Phys. Rev. D* **97** (2018) 035001 [arXiv:1708.09389] [INSPIRE].

JHEP04(2022)024

[87] V.V. Gligorov, S. Knapen, M. Papucci and D.J. Robinson, *Searching for long-lived particles: a compact detector for exotics at LHCb*, *Phys. Rev. D* **97** (2018) 015023 [arXiv:1708.09395] [INSPIRE].

[88] J. Liu, Z. Liu, L.-T. Wang and X.-P. Wang, *Enhancing sensitivities to long-lived particles with high granularity calorimeters at the LHC*, *JHEP* **11** (2020) 066 [arXiv:2005.10836] [INSPIRE].

[89] A. Hook, S. Kumar, Z. Liu and R. Sundrum, *High quality QCD axion and the LHC*, *Phys. Rev. Lett.* **124** (2020) 221801 [arXiv:1911.12364] [INSPIRE].

[90] D. Acosta et al., *Review of opportunities for new long-lived particle triggers in run 3 of the Large Hadron Collider*, arXiv:2110.14675 [INSPIRE].

[91] K.J. Bae, M. Park and M. Zhang, *Demystifying freeze-in dark matter at the LHC*, *Phys. Rev. D* **101** (2020) 115036 [arXiv:2001.02142] [INSPIRE].

JHEP04(2022)024